International Journal of Applied Sciences: Current and Future Research Trends
(IJASCFRT)
ISSN: 2790-3990
https://ijascfrtjournal.isrra.org/index.php/Applied_Sciences_Journal

Impact of Ion Fluence on Ripple Formation Using Ar^+ and Kr^+ Irradiations

Vandana[a*], Aarav Jalan[b], Akshat A Shah[c], Ali Khorakiwala[d], Sananjay Biswas[e], Raj Kumar[f]

[a]*Department of Physics and Astrophysics, Central University of Jammu, Rahya-Suchani, Bagla, 181143, Jammu, India*

[b,c,d,e]*Pion Academy, Shiv Smriti Chambers, Dr Annie Besant Road, Bhim Nagar, Worli, Mumbai, 400018, India*

[f]*Inter University Accelerator Centre, Aruna Asif Ali Marg, New Delhi, 180011, India*

[a]*Email: panchalvandy@gmail.com*

Abstract

This study investigates the impact of altering the fluence of Ar^+ and Kr^+ ion irradiations on the generation of ripples on surfaces. Ar^+ ions with lower mass produces ripples with longer wavelengths due to their higher penetration range compared to Kr^+, but smaller roughness of the ripples is associated with the lower sputtering. The RBS-C investigation indicates that higher ion fluence results in the augmentation of the amorphous layer below the ripples. Mathematical studies validate that as time progresses, the wavelength of ripples expands and is directly related to the length at which atoms are re-deposited, which is determined by the thickness of the amorphous layer. Thus, ripple growth is controlled by solid flow velocity and the amorphous layer's thickness.

Keywords: Ion beam; Ripple patterns; Rutherford backscattering spectroscopy.

Received: 9/15/2024
Accepted: 11/2/2024
Published: 11/15/2024

---

* Corresponding author.

1. Introduction

Ion-beam irradiation (IBI) has been used as an alternative source of nanotechnology in the last few decades to fabricate ordered periodic nanostructures on solid surfaces. IBI techniques have the ability to produce self-organized materials with significant applications in wettability, optoelectronics, quantum devices, and thin films for nano-photonics. These materials include metals, semiconductors, insulators, oxides, and polymers. Under the specific settings of studies, ion irradiations create a variety of nano-scale characteristics, such as dots, ripples, holes, cones, and ditches, such as structures inside typical dimensions of 1–1000 nm [1, 2].The scientific community is becoming interested in the ripple patterns among these nano-scale features because they can be used as a template to modify the three phase (solid-air-liquid) contact line, which will affect the wetting properties of the material. It's interesting to note that the wetting and adhesion characteristics of materials surfaces may be adjusted for a range of purposes by adding particular chemical components to their surfaces.

A target is typically exposed to an intense ion beam (few eV–keV) at a precise oblique incident angle on a solid surface in order to produce the ripple patterns [3]. The shape, size, and regularity of nano-ripples determine many interesting properties of the material; therefore, by varying a number of parameters, such as ion energy [4], ion-fluence [1], flux, and ion-incident angle [5], one can greatly manipulate the surface ripple pattern dimensions (amplitude, wavelength, and size). But in order to advance surface nanotechnology using ion beam sputtering (IBS), a fundamental knowledge of ion-solid interaction is needed. In 1988, Bradley and Harper (BH) introduced a theoretical model that identified the primary mechanism responsible for the formation of ripple patterns under Ion Beam Sputtering (IBS) [3]. The BH theory is essentially derived from Sigmund's theory of sputtering and has proven effective in qualitatively predicting specific length scales in pattern growth and the angular orientation of ripples. It centres on the interplay between two processes: the roughening of the surface due to sputter erosion and the smoothing effect caused by thermal diffusion. This theory provides a qualitative insight into the roles of sputtering and surface diffusion in inducing surface patterning.

2. Experimental Work

Here, we use two distinct projectile masses, Ar+ and Kr+, to analyse the fluence-dependent wavelength of ripples on silicon surfaces. The studies were carried out at the Low Energy Ion Beam Facility (LEIBF) at IUAC New Delhi at room temperature. The ideal incidence angle for ripple generation during ion beam irradiation was 60° relative to the surface normal. At intervals of 2×10^{17} ions/cm^2 ions/cm², the fluence was varied from 3×10^{17} ions cm^2 to 9×10^{17} ions cm^2. For both Ar^+ and Kr^+ ions, the radiation energies were set at 60 keV and 100 keV. Following radiation exposure, AFM in tapping mode was used to examine the surface morphology of Si (100) samples in an ambient setting. Nanoscope software was used to evaluate the data. Furthermore, near-surface damage was evaluated utilising DECADA coding software and Rutherford Backscattering Spectroscopy in channelling mode (RBS-C) [6].

3. Result and Discussion

Figure 1 shows the atomic force microscopy (AFM) images of Si (100) obtained after irradiation by two

different masses of ions Ar^+ and Kr^+ for different energies E = 60 keV and 100 keV. The corresponding z-scale shows the height of surface structures. The experimental work has been carried out for the fluence window of (3-9) $\times 10^{17}$ ions/cm^2 (at a fixed interval of fluence 2 $\times 10^{17}$ ions/cm^2) at fixed angle of 60^o with respect to surface normal for both of ion-beams. Quasi-periodic ripple structures were found to be developed on the surfaces at low fluence of 3 $\times 10^{17}$ ions/cm^2. It seems that the ripples become more homogenous and ordered as soon as there is an increase in the value of ion-fluence (ion-beam time) for both the Ar^+ and Kr^+ ion-beams. The alignment of these ripple patterns are found to be perpendicular to the projection of ion beam direction. The ripples dimensions of irradiated surfaces are presented in Figure. 1(a) and (b), where the wavelength and roughness are found to be function of ion-fluence. The wavelength of ripples increases with increase in ion-fluence after the BH linear regime (linear cascade approximation) [3]. According to BH theory the wavelength of the ripples (λ) remains stabilized during early stage of patterning. In our case the ripple formation observed at lower fluence of 3 $\times 10^{17}$ ions/cm^2 which is found to be grown in wavelength with increase in fluence up to 9 $\times 10^{17}$ ions/cm^2. It is well reported that the wavelength of ripples follow the power law $\lambda \sim f^{\gamma}$ with an exponent $\gamma \leq 1$ due to the non-linear effects at higher ion-fluence. Habenicht and his colleagues [7] also observed similar increase of ripple wavelength with the exponent of 0.50. A non-linear continuum model (hydrodynamic/linear stability) has been successful for explanation of fluence dependence patterning dynamics/parameters. Subsequently, the Kuramoto-Sivashinsky (KS) equation has been proposed for justification of unfamiliar behavior of ripple dynamics which is given as [8]

$$\boldsymbol{d_t h = -v\nabla^2 h - k\nabla^4 h + \lambda^{(1)}(\nabla h)^2 - \lambda^{(2)}\nabla^2(\nabla h)^2} \quad 1$$

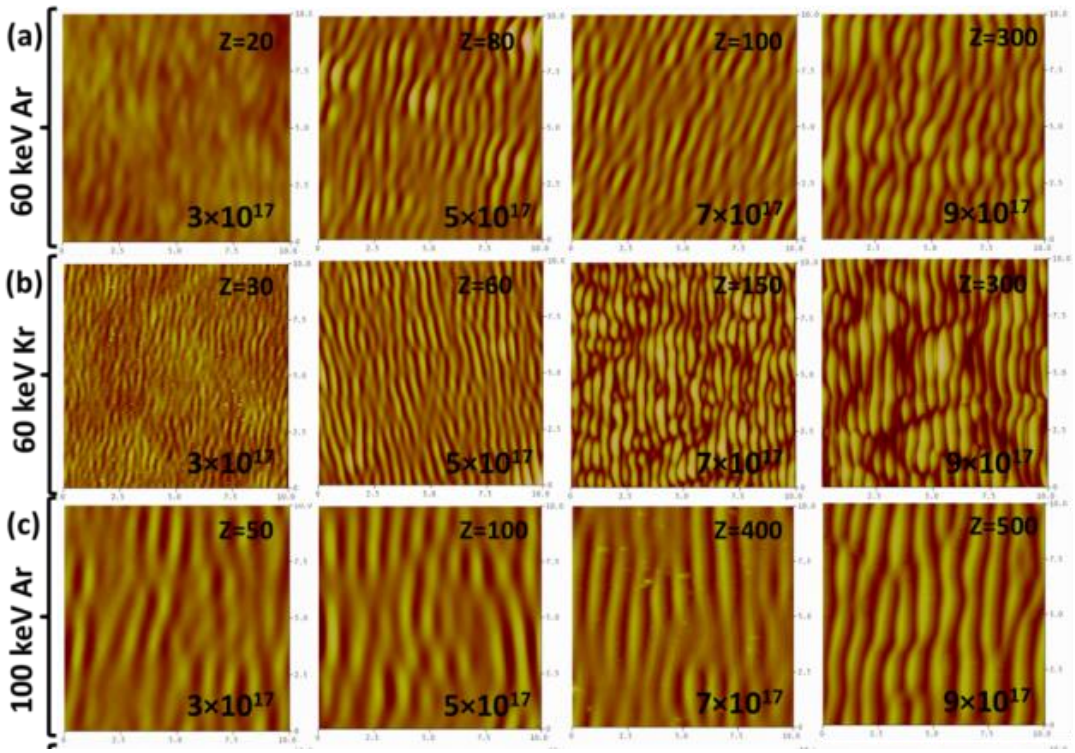

Figure 1: (a-c) AFM images of Ar^+ and Kr^+ ions irradiated substrates of Si(1 0 0) at an angle of 60◦ with respect to surface normal for different ion-fluence of: 3 $\times 10^{17}$,5 $\times 10^{17}$, 7 $\times 10^{17}$ and 9 $\times 10^{17}$ respectively.

Although the non-linear models were not able to identify the co-relation between the ripples wavelength and the depth of near surface damage layer. In recent years, a hydrodynamic model of nanopatterning has been successful to establish this relation. To find this direct co-relation first, the values of roughness and wavelength of ripples for Ar^+ and Kr^+ extracted from AFM images are plotted in figure 2. The roughness's of rippled surfaces are found to be less differentiating at low fluence for two different ion-beams Ar^+ and Kr^+. But at high fluence 9×10^{17} ions/cm^2, the roughness rapidly increases for two different amounts of energies 60kev and 100 keV. Also, the value of rms roughness is found to be higher for 60 keV Kr^+ ion as compared to 60 keV Ar^+ at corresponding irradiated fluences. The values of wavelengths are also found to be different for different ion irradiation parameters. In case of Ar^+ ions the wavelength is much larger in comparison to Kr^+ ion for 60 keV of ion-energy and wavelength is also not the same for same types of ion-masses at two different energies of 60 keV and 100 keV. A direct dependency of wavelength of ripples on ion beam energy proposes to find the wavelength dependency upon the ion penetration depth. This higher roughness and lower wavelength of ripples in case of Kr^+ than Ar^+ not only depends upon the sputtering of the target but also on the mass flow. First, to find a relation between the ripples wavelength and the thickness of amorphous layer the role of sputtering and solid mass flow are confirmed through the power spectral density (PSD) study as follows.

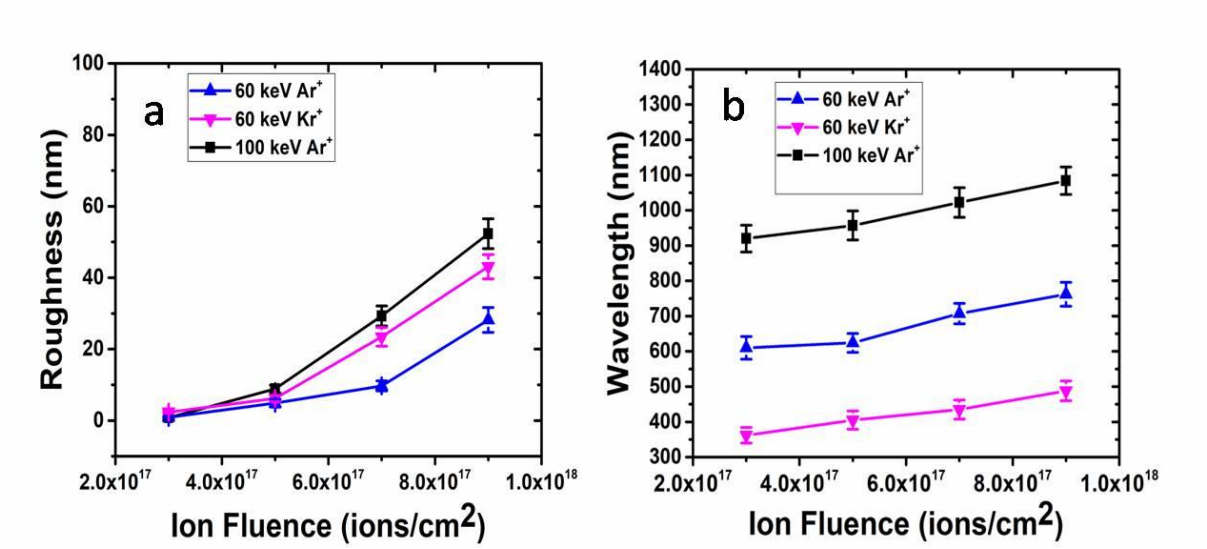

Figure 2: Variation in wavelength (a) and roughness (b) with ion-fluence for two different projectiles of masses Ar^+ and Kr^+.

Two methods may be used to qualitatively estimate the roles of mass diffusion and sputtering in ion beam sputtering (IBS) driven surface patterning: (a) Power Spectral Density (PSD) analysis; and (b) visualising the ripples' wavelength as a function of ion beam energy. A Fourier transform of the surface, the PSD function is defined as follows [9]:

$$PSD = \frac{1}{A}\left[\frac{d^2r}{2\pi}e^{ikr\langle h(r)_t\rangle}\right]^2 \qquad 2$$

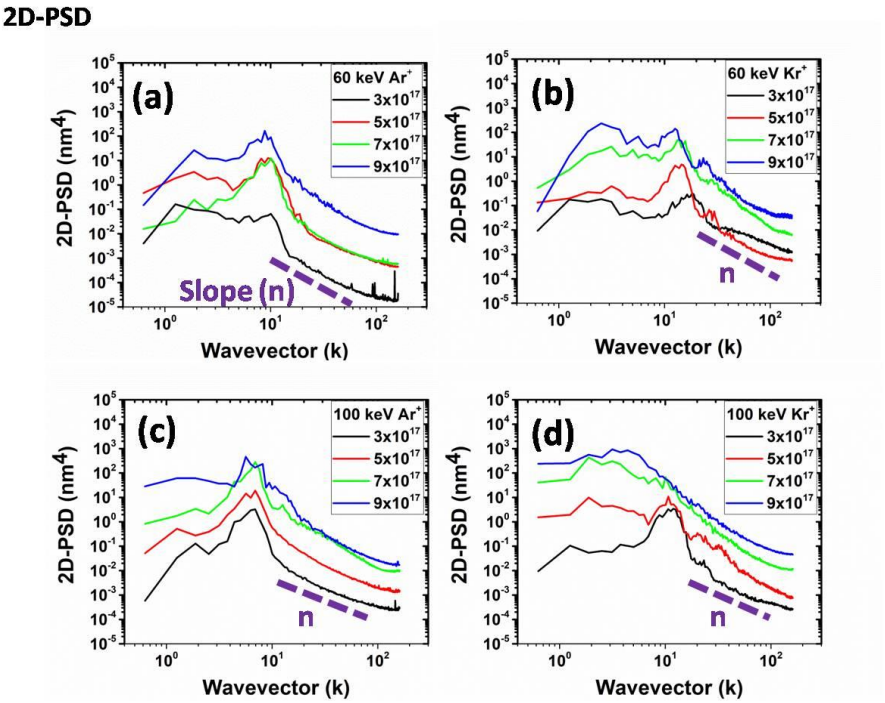

Figure 3: 2D Power spectral density (2D-PSD) as a function of wave-vector.

where (k) is the spatial frequency (nm^{-1}), $h(r)$ is the surface height at any given position 'r'on the surface, and A is the surface area. Our experimental results show that the PSD function may be directly retrieved from AFM pictures (see Figure 3). The PSD typically exhibits a power-law dependency in the high-frequency regime, PSD = k^{-n}, where n is a real number representing surface alterations brought on by surface diffusion and sputtering. Additionally, by using the formula $\alpha = (n-d)/2$, where 'd' is the PSD plot's dimension—which is taken to be two for this study—the roughness exponent 'α' may be computed from the PSD function.

If the value of α falls in the range of the 0.66-1, the surface diffusion process would be expected whereas if α is less than 0.5 then the surface mobility is not allowed [9]. Slope values are found to be lower for low irradiated fluences. Extracted values of roughness exponent α have the range of 0.5-0.75 for all thicknesses at high fluence 9×10^{17} ions/cm^2, which are higher (α = 0-0.35) than that at lower fluences. So, it can be concluded that the irradiation at higher fluences is governed by mass flow processes. According to hydrodynamic model of mass flow there is a relationship between the ion penetration depth i.e. thickness of the amorphous layer with energy E, as $d = E^{2m}$ and where the typical values of 'm' lie in-between 1/3 and 1/2 as determined from TRIM [11]. Based on this assumption, the wavelength of ripples is derived in terms of thickness of amorphous layer. In our experimental work, the thicknesses of amorphous layer have been determined using Rutherford backscattering measurements. Figure 4 (a), (b) and (c) show the RBS spectra of irradiated samples in channeling mode at 60 keV Kr^+, 60 keV Ar^+, and 100 keV Ar^+, respectively at different fluences. Corresponding damage profiles extracted from DECADA software are also presented in the right column. Full width at half maximum (FWHM) of damage profile is used to calculate the penetration damage range of corresponding ion. The observed depth of damage or amorphous silicon (a-Si) is nearly ~ 66-70 nm for 60 keV Kr^+ ion beam, which is comparatively lower than ~100-106 nm for 60 keV Ar^+. This suggests that the observation of larger wavelength of ripples for

60 keV Ar+ is due to larger penetration depth of Ar as compared to Kr. To confirm this observation, the damage depth has also been investigated for 100 keV Ar^+, which are found to be ~147-154 nm. This confirms the observation of higher wavelength of ripples for 100 keV Ar+ as compared to 60 keV Ar^+ and Kr^+ ions.

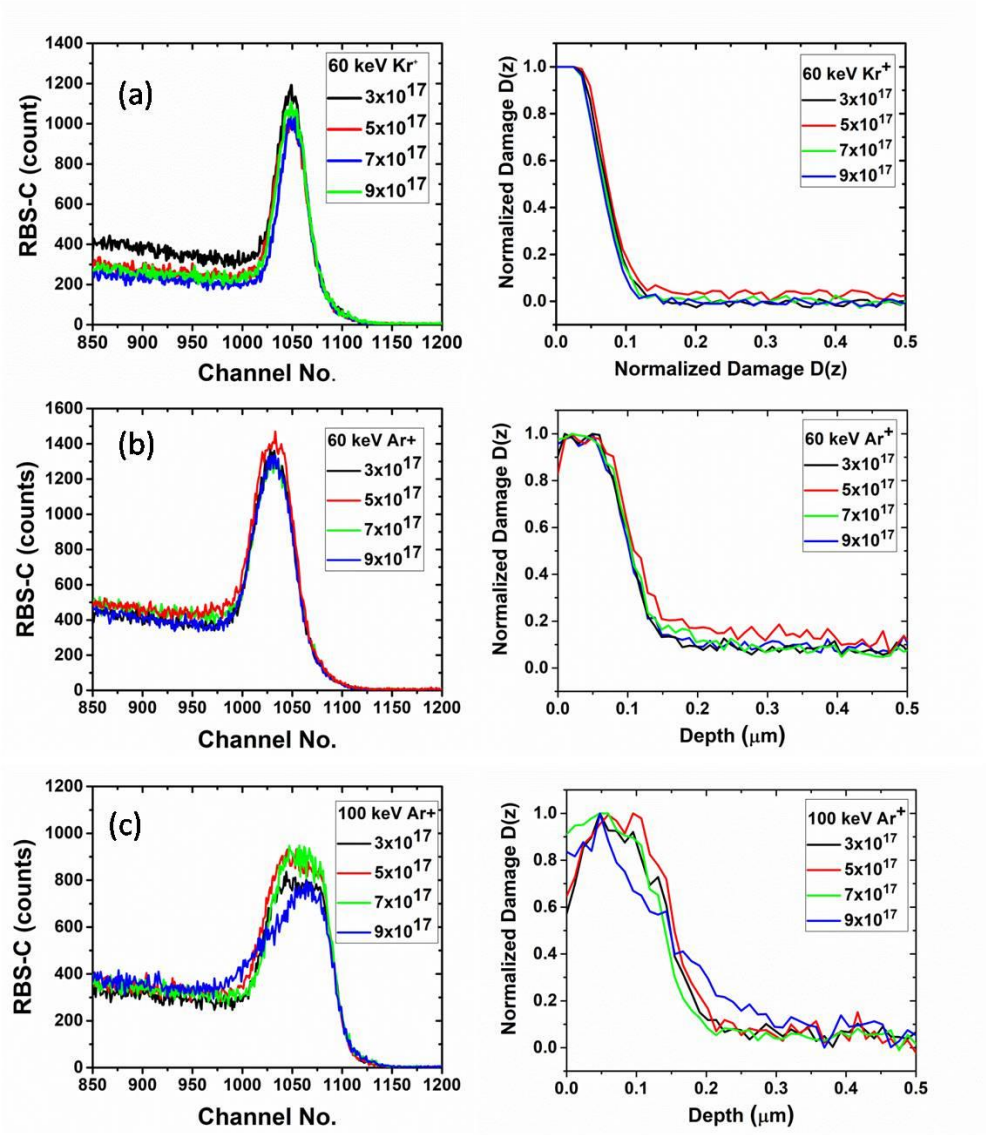

Figure 4: Rutherford backscattering spectra in channeling mode: (a) 60 keV Kr^+, (b) 60 keV Ar^+ and (c) 100 keV Ar^+. Corresponding Damage profiles are shown in right column.

To establish a co-relation between ripples wavelength (λ) and average thickness of amorphous layer (Ta), all the extracted values of rms roughness, wavelength of ripples and thickness of amorphous layer were presented in table 1. A ratio of average wavelength (λ) of ripples to average thickness of amorphous layer (Ta) is presented in the last column. It could be seen that the ratio λ/Ta is 6-7.3 for 60 keV Ar+ and 5.6-7.17 for 60 keV Kr^+. It is concluded that the wavelength is found to be proportional to thickness of amorphous layer with proportionality constant varying from ~6 to 7.

Table 1: Different surface morphological and ion-beam parameters (estimated from SRIM-TRIM, [1]) at different energies of Ar^+ and Kr^+.

Ion beam	Energy	Parameters					
		Sputtering Yield (*Y*) (atoms/ion)	Rms roughness (R)	Thickness of Amorphous layer (T)	Average thickness (T_a)	wavelength	Wavelength/a-layer thickness (λ/T_a)
Ar^+	*60*	7.4	1.33±0.06	100-106	103	610-762	6-7.3
	100	6.7	15.2±0.76	147-154	148	920-1084	6.2-7.3
Kr^+	*60*	14.5	23.9±1.20	66-70	68	382-488	5.6-7.17

4. Mathematical modeling of ripples formation

4.1 Methods of modeling

In this section, we have the radical assumption of solid flow resulting in erosion and re-deposition of silicon atoms at the a/c interface. The incompressible solid mass flow inside the amorphous layer results in the formation of ripple structures at the a/c interface, which are also manifested at the free surface. This assumption is identical to the process of saltation in formation of macroscopic ripples on sand dune under air blow [10, 11]. To understand the mechanism(s) of ripples formation, here, we assumed that the solid flow velocity ($V_s^{x,y}$) inside the amorphous layer controls the re-deposition length ($l_{s(x,y)}(x,y)$ of silicon atoms. And, the amount of mass transport (q_o) can be assumed to be higher for higher mass of ion irradiation. Keeping in mind all these assumptions, we can formulate the process of re-deposition of Si atoms in the following discrete mathematical equations:

Re-deposition: The process of re-deposition can be described by following equations [10]:

$$h^{'}(x,y) = h(x,y) - q_s(x,y) \quad (3)$$

$$h'(x + l_{sx}, y + l_{sy}) = h(x + l_{sx}, y + l_{sy}) + q_s(x,y) \quad (4)$$

$$\vec{l}_s(x,y) = l_{sx}(x,y)\vec{i} + l_{sy}(x,y)\vec{j} \quad (5)$$

$$q_s(x,y) = q_0 + c\tanh(g(x,y))) \quad (6)$$

Where $h(x,y)$ and $h'(x,y)$ are the surface heights at a point (x,y) on a/c interface before and after mass re-deposition, respectively. $\vec{l}_s(x,y)$ stands for the re-deposition length along the ion beam projection vector, $q_s(x,y)$ is the amount of materials of silicon transferred, q_0 is a minimum base value of silicon, $g(x,y)$ is a function of the gradient of a/c surface at point (x,y), defined as:

$$g(x,y) = sign\left(\frac{\partial h}{\partial x}\right)\sqrt{\left(\frac{\partial h}{\partial x}\right)^2 + \left(\frac{\partial h}{\partial y}\right)^2} \qquad 7$$

The picked up silicon atoms by the solid flow are deposited at a minimum length is proportional to the velocity of solid flow. Castro *and his colleagues* [12, 13] and Kumar *and his colleagues* [14] have already formulated the role of solid flow in growth and formation of ripples. With all these assumptions we can define the solid flow velocity inside the amorphous layer ($V_s^{x,y}$) as a function of re-deposition length ($l_{s(x,y)}(x,y)$) as:

$$V_s^{x,y} = V_o[1 - \tanh(\frac{\partial h}{\partial x})] \qquad 8$$

$$l_{s(x,y)}(x,y) = (l_0)V_s^{x,y} \qquad 9$$

where V_o and l_0 are the initial velocity and re-deposition length control parameters, and

$\frac{\partial h}{\partial x}$ and $\frac{\partial h}{\partial y}$ are the slopes in *x* and *y* directions, respectively.

Smoothening: Smoothening is the process of suppressing and flattening of ripples growth at a/c interface, and can be described by:

$$h_{n+1}(x,y) = h_{n'}(x,y) + D\left[\frac{1}{6}\sum_{NN} h_{n'}(x,y) + \frac{1}{12}\sum_{NNN} h_{n'}(x,y) - h_{n'}(x,y)\right] \qquad 10$$

where, $\sum_{NN} h_{n'}(x,y)$ and $\sum_{NNN} h_{n'}(x,y)$ represent the summation of the heights of the adjacently horizontal,

vertical and diagonal sites; and *D* is a relaxation factor [11].

4.2 Mathematical modelling

In context of experimental results the discrete mathematical simulation has been performed using the above formalism for different values of initial re-deposition length (l_o) as a function of run steps. Initial values of re-deposition length (l_o) is driven by the initial velocity (V_o) of solid flow inside the amorphous layer, which are

functions of ion beam irradiation parameters. Radically we have assumed that the higher penetration range of higher energies of Ion beam results in higher re-deposition length. This assumption is supported by the experimental observation of larger wavelength of ripples for higher energies of Ar ion beam. Simulation has been performed for three different l_o = 5, 7.5 and 10 values as a function of run steps, which correspond to experimental variation of amorphous layer thickness, as shown in Figure 5 (a-c). Other parameters have been fixed such that V_o = 20, a = 0.1, c = 0.1, q_o = 0.1. Following the simulation, observed wavelength values are displayed in Figure 5 (d), which exhibit the same pattern as the observed experimental values of the fluence dependent investigation for various ion beam energies of Ar and Kr in the previous section. For comparison with the simulation results, fluence-dependent wavelengths of ripples have also been presented in Figure 5 (e). These simulation studies show that the wavelength of ripples is a function of ion beam energy or the thickness of amorphous layer. Higher thickness of amorphous layer is found to be more favourable for the formation of longer wavelength of ripples. Thus the re-deposition length of silicon atoms at the a/c interface controls the wavelength of ripples which has also been observed in macroscopic world [10, 11]. Although the idea of re-deposition of silicon atoms at the a/c interface in ripples formation has not been considered by several groups due to higher density of the mass flow inside the amorphous layer [12, 15, 16]. Nevertheless the assumption of the ripple formation occurs at the a/c interface due to mass flow inside the amorphous layer, all phenomena like ripples growth and propagation etc. can be correlated with irradiation ion beam parameters.

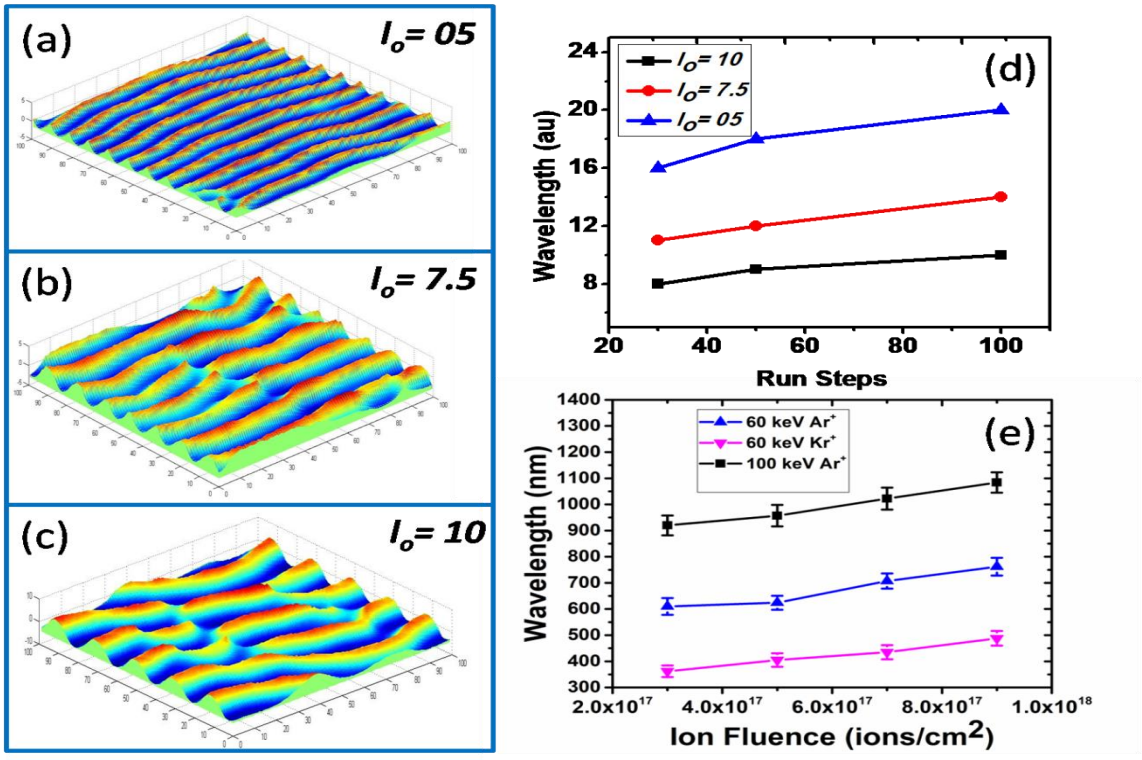

Figure 5: (a-c) Simulation results for parameters V_s=20, a=0.1, c=0.1, q_o =0.1 for different values of l_o=5, 7.5 and 10, respectively, at 100 run steps. (d) Plot of wavelength as a function of run-step for different values of l_o. (e) Plot of the wavelength of ripples as a function of ion fluence at different incident ion energy.

5. Conclusions

This work shows that ripple development on surfaces is strongly influenced by the fluence of Ar^+ and Kr^+ ion irradiations. Ar^+ ions have longer wavelength ripples but less roughness because of less sputtering, which is caused by their lower mass and greater penetration range. RBS-C analysis shows that the thickness of the amorphous layer underneath the ripples increases with increasing ion fluence. The amorphous layer thickness determines the re-deposition length of atoms, which is strongly correlated with the increasing ripple wavelength over time, as shown by mathematical models. As a result, the solid flow velocity and the amorphous layer thickness largely govern the development of ripple patterns.

Acknowledgements

Authors acknowledge the India Sulania, IUAC, New Delhi for carrying out the work.

6. Conflict of interest

Authors have no conflict of interest with any work.

References

[1]. Gupta, D., et al. Ripple pattern formation on silicon carbide surfaces by low-energy ion-beam erosion. in Journal of Physics: Conference Series. 2023. IOP Publishing.

[2]. Kumar, T., et al., Nano-pits on GaAs (1 0 0) surface: Preferential sputtering and diffusion. Nuclear Instruments and Methods in Physics Research Section B: Beam Interactions with Materials and Atoms, 2016. **379**: p. 52-56.

[3]. Bradley, R.M. and J.M. Harper, Theory of ripple topography induced by ion bombardment. Journal of Vacuum Science & Technology A: Vacuum, Surfaces, and Films, 1988. **6**(4): p. 2390-2395.

[4]. Vandana, et al., Energy-dependent surface nanopatterning of Si (100) for different projectiles: a tunable anisotropic wettability of ripple surface. Applied Nanoscience, 2021: p. 1-8.

[5]. Rauschenbach, B., Low-Energy Ion Beam Bombardment-Induced Nanostructures, in Low-Energy Ion Irradiation of Materials: Fundamentals and Application. 2022, Springer. p. 305-405.

[6]. Stamp, G., et al. DECADA: Tool for discrete-event control and diagnosis analysis. in 2006 8th International Workshop on Discrete Event Systems. 2006. IEEE.

[7]. Habenicht, S., et al., Ripple propagation and velocity dispersion on ion-beam-eroded silicon surfaces. Physical Review B, 2002. **65**(11): p. 115327.

[8]. Rost, M. and J. Krug, Anisotropic Kuramoto-Sivashinsky equation for surface growth and erosion. Physical review letters, 1995. **75**(21): p. 3894.

[9]. Elson, J.M. and J.M. Bennett, Calculation of the power spectral density from surface profile data. Applied optics, 1995. **34**(1): p. 201-208.

[10]. Nishimori, H. and N. Ouchi, Formation of ripple patterns and dunes by wind-blown sand. Physical Review Letters, 1993. **71**(1): p. 197-200.

[11]. Miao, T.-D., Q.-S. Mu, and S.-Z. Wu, Computer simulation of aeolian sand ripples and dunes. Physics

Letters A, 2001. **288**(1): p. 16-22.

[12]. Castro, M. and R. Cuerno, Hydrodynamic approach to surface pattern formation by ion beams. Applied Surface Science, 2012. **258**(9): p. 4171-4178.

[13]. Castro, M., et al., Stress-induced solid flow drives surface nanopatterning of silicon by ion-beam irradiation. Physical Review B, 2012. **86**(21): p. 214107.

[14]. Tanuj Kumar, A.K., N. P. Lalla, Sonu Hooda, Sunil Ojha, Shammi Verma, and D. Kanjilal, To be submitted.

[15]. Bradley, R.M. and J.M.E. Harper, Theory of ripple topography induced by ion bombardment. Journal of Vacuum Science & Technology A: Vacuum, Surfaces, and Films, 1988. **6**(4): p. 2390-2395.

[16]. Norris, S.A., et al., Molecular dynamics of single-particle impacts predicts phase diagrams for large scale pattern formation. Nature communications, 2011. **2**: p. 276.